HHS Public Access

Author manuscript

Analyst. Author manuscript; available in PMC 2018 October 23.

Published in final edited form as:

Analyst. 2017 October 23; 142(21): 4018–4029. doi:10.1039/c7an01001j.

Applications of vibrational tags in biological imaging by Raman microscopy

Zhilun Zhao[1], **Yihui Shen**[1], **Fanghao Hu**[1], and **Wei Min**[1,2,3,*]

[1]Department of Chemistry, Columbia University, New York, 10027

[2]NeuroTechnology Center, Columbia University, New York, 10027

[3]Kavli Institute for Brain Science, Columbia University, New York, 10032

Abstract

As a superb tool to visualize and study the spatial-temporal distribution of chemicals, Raman microscopy has made big impacts to many disciplines of science. While the label-free imaging has been the prevailing strategy in Raman microscopy, recent development and applications of vibrational/Raman tags, particularly when coupled with stimulated Raman Scattering (SRS) microscopy, have generated intense excitement in biomedical imaging. SRS imaging of vibrational tags has enabled researchers to study a wide range of small biomolecules with high specificity, sensitivity and multiplex capability, at single live cell level, tissue level or even *in vivo*. As reviewed in the article, this platform has facilitated imaging distribution and dynamics of small molecules such as glucose, lipids, amino acids, nucleic acids, and drugs that are otherwise difficult to do with other means. As both the vibrational tags and Raman instrumental development progress rapidly and synergistically, we anticipate that the technique will shed light onto an even broader spectrum of biomedical problems.

Graphic abstract

In this article, we review the recently successful applications of SRS and vibrational tags on biological problems.

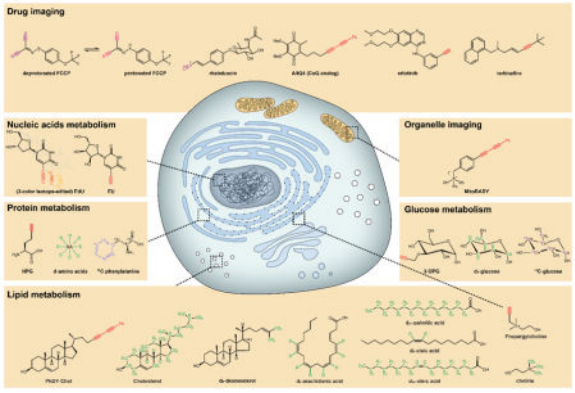

*Corresponding author. wm2256@columbia.edu.

Introduction

Directly visualizing biological structures and activities at cellular and sub-cellular level remains one of the most intuitive and powerful ways to study biological problems by far.[1] Ever since the first microscope was invented in the 17th century, which led to the discoveries of cells and laid the very foundation of the modern understanding of biology, the field of optical microscopy has been advancing rapidly. The emergence of new tools and techniques such as confocal microscopy, super-resolution microscopy and nonlinear microscopy etc. has made it possible for scientists to see and study biology in a noninvasive manner with high spatial-temporal resolution, and thus has expanded our knowledge in life sciences. Among these methods, stimulated Raman scattering (SRS) microscopy, is a powerful tool that can generate image contrast of vibrational transitions of chemical bonds with high sensitivity, resolution and speed[2–4]. Unlike fluorescence microscopy, which generally requires the target to be labeled with a relatively bulky fluorophore, SRS microscopy requires no label or only minimal labels that better preserve the structure and function of the small molecules and are more resistant to photobleaching. When compared to another Raman imaging technique, Coherent anti-Stokes Raman spectroscopy (CARS), SRS is also free from non-resonant background and has linear signal dependence on analyte concentration, which makes it well suited for quantitative studies that are of immense importance for answering biological questions.[5, 6]

Label-free imaging has long been adopted for SRS microscopy and vibrational imaging in general, because it doesn't require any exogenous labeling and reflects native cellular metabolic states.[7–9] The very nature of label-free imaging techniques permits such applications to be performed *in vivo*. Chemical bonds such as O–P–O, C═O, C═C, S═O, O–H, C–H are frequently probed, especially C–H as it is highly enriched in lipids and proteins – the most abundant biomolecules in the cell – and thus gives the highest signal. More importantly, the rich spectral features that vary between different molecules makes it possible for hyperspectral imaging of multiple chemical species that are always of great interest to biologists. In recent advances with label-free techniques, for example, metabolic heterogeneity of live *Euglena gracilis* has been studied[10], providing insight to microalgal research; in other studies, neurotransmitter[11] and neuronal membrane potential[12] have been visualized, adding new tools to investigate neurobiology; and brain tumor infiltration diagnostics[13, 14] has been successfully demonstrated in mouse brain and human patient samples, and an intraoperative set-up using fiber laser was then engineered[15] to assist surgery. However, although label-free vibrational imaging has been demonstrated a useful tool in biological studies, the detection specificity is usually limited – any molecules that harbor the same chemical bond of target will have severely overlapping spectrum and make it extremely hard to image a specific molecule of interest.

For the above reason, Raman/vibrational tags have been developed to circumvent the endogenous cellular background and enable specific detection of the chemical species of interest. This is achieved by introducing chemical bonds that vibrate in the cell-silent Raman window (1800 – 2600 cm^{-1}), in which no endogenous molecules vibrate. There are several benefits associated with using vibrational tags. Stable isotope substitution (such as ^{2}H and ^{13}C) has been long exploited in NMR, mass spectroscopy and Raman spectroscopy. The

substituted molecules are almost chemically identical to the unsubstituted, and thus have good metabolic labeling efficiency. Another alternative is to label molecules of interest with tiny vibrational tags such as nitrile and alkyne. These tags also have unique vibrational frequencies in the cell silent window, and have much larger Raman scattering cross sections to generate strong signal, which is another major advantage of using vibrational tags. Generally, two labeling strategies are associated with these labeled molecules: steady-state or pulse-chase labeling. For the steady-state strategy, labeled molecules are added long enough until the incorporation approaches steady-state, and information such as spatial distribution and incorporation rate can be obtained; while for the pulse-chase labeling strategy, labeled molecules are added for a certain amount of time and then removed, and the decay of the tags can be traced to provide additional turnover kinetics. By these methods complex dynamic information could be obtained which is hard to extract from label-free approach. Furthermore, the introduced vibrational tags can be manipulated in terms of vibrational frequencies, which makes multi-color imaging feasible. There are advantages and disadvantages associated with stable isotope substitution and tiny vibrational tags. Isotope substitutions are chemically identical to the original forms, and the kinetic isotope effect is usually negligible for the duration of typical experiments. Thus, the incorporation to their metabolites is the same as the original forms. But the Raman cross sections of these tags are small, and the signal from these tags is weak. For the above reasons, isotope substitution is ideal for imaging small but abundant biomolecules that are easily perturbed by structural alteration. Other vibrational tags such as alkyne on the other hand usually have much larger Raman cross sections, and yield a large signal at low concentration. Yet the alkyne moiety introduces structural alternation to the molecules and could potentially alter the chemical activity[16]. And therefore it is usually necessary to test the bioactivity when labeling a molecule with alkyne moiety.

In this article, we review recent applications of Raman imaging with vibrational tags, with an emphasis on SRS, on life sciences such as cellular metabolism of nucleic acid, protein, lipid, glucose, small molecule imaging such as drug, and organelle imaging, as well as brain and tumor metabolism. We hope we can convey the potential of SRS imaging of vibrational tags on biological studies especially the ones focusing on cellular metabolism and small molecule imaging.

Nucleic Acid Metabolism

In this section, we review the application of vibrational tags to interrogate nucleic acid metabolism. Conventionally nucleic acids can be visualized by helix-intercalating dyes such as DAPI or Hoechst or hybridization-based techniques. However, metabolic imaging of nucleic acids reveals more information on the dynamic aspect, which is dependent on cell activity. For example, new DNA synthesis reflects cell proliferation, while the RNA turnover is considered as a regulatory control over protein level. Traditionally, measuring DNA synthesis was achieved by nucleoside analog bromodeoxyuridine (BrdU), which can then be detected using antibody against BrdU. Later, the development of bioorthogonal chemistry introduced alkyne as a chemical handle into a deoxyuridine (dU) analog, 5-ethynyl deoxyuridine (EdU)[17]. However, these methods either cannot work with live cells, or suffer from non-specific membrane staining background.

Raman imaging is then recognized as the suitable tool to visualize the alkyne-tagged nucleoside analogs without further modification or click-chemistry reaction. Along this, Yamakoshi *et al.* demonstrated imaging of EdU incorporated in DNA by spontaneous Raman micro-spectroscopy in living cells[18] (Figure 1A). To further boost the imaging speed and sensitivity and achieve live cell imaging, Wei *et al.* and Hong *et al.* independently applied stimulated Raman scattering and captured the newly synthesized DNA in living cells[19, 20] (Figure 1B–C). Wei *et al.* also successfully probed cell proliferation in *C. elegans* germline[19] (Figure 1D). Later Chen *et al.* created different vibrational colors for EdU by isotope-editing the alkyne moiety[21] (Figure 1E–F). With these multi-color labels and applying them in a pulse-chase manner, Hu *et al.* recently showed that even different stages of DNA synthesis could be visualized in the same nuclei of neural progenitor cell[22] (Figure 1G–I). Thus, the live-cell imaging capability of SRS as well as the multiplexing potential of EdU makes it possible to reveal cell cycle dynamics in complex tissue or animal samples.

Using the similar strategy, RNA synthesis can be measured by incorporation of alkyne-tagged uridine analog, 5-ethynyl uridine (EU)[23]. Employing SRS imaging, Wei *et al.* visualized RNA synthesis, most of which is attributed to ribosomal RNA[19]. With pulse-chase labeling, they also showed that compared to DNA dynamics at the time scale of a cell cycle, RNA turnover is much faster (Figure 1J).

Protein Metabolism

As the last piece in central dogma, protein metabolism is tightly controlled via both synthesis and degradation. Some modalities of measuring protein dynamics have been developed, such as genetically encoded GFP reporter[24] and SILAC-based protein mass spectrometry[25]. The former fuses GFP to a specific protein, which enables fluorescence imaging and quantification of one protein at a time[24]. It allows spatial information to be obtained in live cells, but is only limited to selected proteins and does not report the global protein homeostasis. The latter uses isotope-labeled amino acids to create mass shift in peptides, which marks the newly synthesized proteins in mass spectrometry[25]. It provides rich information of a large number of proteins at the same time, yet losses the spatial resolution when working with cell lysate. Complementary to the above modalities, in this section we summarize how Raman imaging of vibrational tags can be applied to interrogate protein metabolism. The vibrational tags are introduced to amino acids, which can then be metabolically incorporated into proteome after pulse and/or chase labeling. It offers spatial information of global proteome dynamics in live cells, which would be valuable under scenarios such as local protein synthesis and dysfunction of protein quality control system.

Similar to alkyne tagged nucleic acids, alkyne has also been introduced to amino acids in a methionine analog, HPG[26]. Although HPG suffers from low incorporation rate compared to natural methionine (~1/1000), Wei *et al.* and Hong *et al.* were still able to visualize protein synthesis using highly sensitive SRS microscopy[19, 20] (Figure 2A). Alternatively, isotope-labeled (^{2}H- or ^{13}C-) amino acids can be used. The carbon-deuterium bond enriched in newly synthesized proteins serves as a good Raman-active analogue in the cell-silent region. van Manen *et al.* imaged protein synthesis using d_5-phenylalanine with spontaneous Raman microspectroscopy[27]. Wei *et al.* further improved the label incorporation using a mixture of

20 deuterated amino acids, and applied SRS for fast image acquisition[28] (Figure 2B–E). This methodology is later optimized into a general platform to interrogate protein metabolism across a variety of systems, including primary neuron cells, brain tissues, and even whole animals including zebrafish larvae and mouse[29] (Figure 2F and G). They revealed possibly function-related higher protein synthesis activity in hippocampus and cortical regions in a brain slice. Moreover, employing the spectral difference between two subsets of deuterated amino acids, they were also able to image two temporally distinct populations of newly synthesized proteins.

Apart from protein synthesis, isotope-labeled amino acids could also provide information for protein degradation. This is achieved by imaging the signal decay of the 'old' proteome. Shen *et al.* measured the decay of the endogenous phenylalanine peak after ^{13}C-phenylalanine labeling to map protein turnover under both steady state and stressed conditions[30] (Figure 2H–J). In this way, heterogeneous population was observed for perturbed protein turnover in a model for neurogenerative disease. Interestingly, they found that in cells with large huntingtin protein aggregation, the overall proteomic turnover remains normal. However, in cells with oligomeric huntingtin protein, reduced proteomic turnover can be observed, suggesting the oligomeric but not aggregated huntingtin as the toxic species (Figure 2I and J).

Lipid Metabolism

Lipids are indispensable biomolecules that function in energy storage, membrane architecture and signaling. They consist of a variety of molecules. For example, triacylglyceride and cholesterol ester are the major lipids stored in lipid droplets; cholesterol is a major component in plasma membrane; the amphipathic phospholipids make up most of the cell membrane. To study lipid metabolism, vibrational tags could be introduced into the precursor or building blocks. Enrichment of tags into the newly synthesized lipids could offer contrast for imaging. In this section, we will summarize the applications of vibrational tags in studying metabolisms of cholesterol, fatty acids and choline. For more general reviews about applications of Raman imaging in lipid biology, the readers could refer to earlier reviews by Yu *et al.*[31] and Syed *et al.*[32]

Cholesterol is a well-known regulator of membrane biophysical properties, thus its concentration and subcellular distribution are critical for membrane protein functions and signaling. Excess cholesterol can be stored in lipid droplets as cholesterol ester or degraded by oxidation. Disturbed cholesterol metabolism is associated with many diseases such as Niemann-Pick type C (NPC) and atherosclerosis[33]. Thus, there is an increasing need for quantitative imaging of cholesterol distribution as well as its metabolism. Towards this purpose, filipin has been used as naturally fluorescent cholesterol-binding probe. Yet it remains undetermined whether it authentically reports cholesterol distribution[34]. Fluorescent analogs of cholesterol such as dehydroergosterol and NBD-cholesterol were developed previously for such purpose, yet the former requires UV excitation while the latter inevitably changes the physicochemical properties of cholesterol[34].

In this case, Raman imaging enables the use of small tags that better preserve the identity of cholesterol. Indeed, several reports have successfully applied Raman imaging to study cholesterol metabolism. For example, cholesterol isotopologues with different number of deuterium substitutions have been used (Figure 3A). Specifically, Matthäus *et al.* have used d_6-cholesterol with spontaneous Raman imaging to reveal LD accumulation of cholesterol scavenged by macrophages[35] (Figure 3B). Alfonso-Garcia *et al.* improved the labeling density by using d_{38}-cholesterol purified from an engineered yeast strain[36] (Figure 3A). With SRS imaging, they were able to reveal heterogeneous partitioning of free cholesterol, cholesterol ester and triglyceride into LDs (Figure 3C and D). In another study[37], d_6-desmosterol was found accumulated in LDs when the cells were infected by hepatitis C virus.

To further boost the detection sensitivity, Lee *et al.* synthesized a phenyldiyne-tagged cholesterol analog[38] (Figure 3E). Phenyldiyne (conjugated two alkynes terminated by a phenyl group) has even larger cross-section than single alkyne (15 times), and approximates to 20 fully deuterated cholesterol molecules. Although phenyldiyne is more perturbative than the minimal labeling by deuterium, its larger cross-section enables visualization of cholesterol in not only LDs, but also in lysosomes and membrane (Figure 3F and G). The authors also showed that phenyldiyne-tagged analog resembled the behavior of natural cholesterol, including esterification-dependent accumulation in LDs, lysosomal accumulation in an NPC disease model, as well as protein-dependent uptake in *C. elegans* (Figure 3H).

Phospholipids comprise the majority of the membrane structures, and choline is among the most abundant head groups for phospholipids[39]. Choline immobilization in cell reflects mainly membrane synthesis activity. To visualize this process, Hu *et al.* has applied d_9-choline in a variety of cell types including primary mouse neurons to image choline metabolites with SRS[40]. With this, they were able to reveal the elevated choline metabolism in cancer cells and highlighted the importance of choline in embryogenesis (Figure 3I–K). To improve detection sensitivity, Lu *et al.* adopted an alkyne-tagged choline analog, propargylcholine[19]. With the shifted alkyne frequency in the positively charged choline, they also demonstrated two-color imaging of choline metabolism (propargylcholine) and DNA synthesis (EdU).

Fatty acids not only serve as an energy source for cells through oxidation, but also build up the hydrophobic part of the membrane, while excess fatty acids are stored in LDs. The metabolic flow of fatty acid is dynamically regulated to maintain lipid homeostasis. Thus, the acquisition of spatiotemporal information of lipid metabolites provides insight into how this regulation is accomplished. Towards this goal, Raman-active analogues of fatty acids have been used, namely deuterium-labeled fatty acids and alkyne-labeled fatty acids. For example, van Manen *et al.* used d_8-arachidonic acid (AA) to label LDs in neutrophils, and observed close association between AA-enriched LDs and phagosome[41]. Xie *et al.*[42] and Weeks *et al.*[43] demonstrated that d_{33}-oleic acid or d_2-oleic acid could be used for CARS microscopic imaging of lipid droplet. With reduced non-resonant background in SRS, Zhang *et al.* were able to reveal the cellular uptake of d_{31}-palmitic acid and its incorporation into LDs and membrane[44]. Matthäus *et al.* used d_{31}-palmitic acid and d_{33}-oleic acid to quantify

the fatty acid scavenging kinetics in human macrophages by Raman spectroscopic imaging[35]. Recently the same group applied SRS imaging with faster speed and revealed heterogeneous uptake dynamics across the cell population[45]. Not all fatty acids are metabolized in the same way. To reveal the 'metabolic fingerprinting' of fatty acids, Fu *et al.* applied hyperspectral SRS imaging for neutral lipid profiling[46]. The spectral signatures in different fatty acids, including d_{31}-palmitic acid, d_{33}-oleic acid, and d_8-arachidonic acid, allowed simultaneous tracking of their incorporation (Figure 3L–O). Alkyne-tagged analogs can also be used for tracking fatty acid metabolism. For example, Wei *et al.*[19] demonstrated imaging of 17-octadecynoic acid, a palmitic acid analog, that was scavenged by macrophages or taken up by C. elegans. Hong *et al.*[20] also showed the same molecule incorporated into LDs.

Glucose metabolism

Glucose is the primary energy source for almost all living organisms, and cells actively regulate glucose metabolism to support cell functions. Therefore, regional glucose uptake is an indicator of tissue metabolic activity, and is used as a diagnostic contrast[47]. To achieve such goals quantitatively, glucose analogues have been adopted in imaging and diagnostic techniques such as positron emission tomography (PET) and magnetic resonance imaging (MRI)[48]. For example, PET tracers such as ^{18}F-fludeoxyglucose (^{18}FDG) are widely used in clinical diagnostics, and recently MRI of glucose has been demonstrated by chemical exchange saturation transfer and hyperpolarization of ^{13}C labeled glucose. However, both PET and MRI have limited spatial resolution and cannot visualize glucose uptake in single cells. Fluorescent analogs such as 2/6-NBDG have thus been developed to achieve optical resolution.[49, 50] But the large physical size and the hydrophobicity of the fluorophores significantly influence the property of natural glucose and could cause non-specific interactions in cells and tissues[51, 52].

A novel glucose analogue 3-O-propargyl-d-glucose (3-OPG) has been recently developed to visualize glucose uptake activity in single cells by SRS[16] (Figure 4A). A small alkyne tag was introduced onto glucose molecule to provide a strong and characteristic Raman signal in the cell-silent window and can be imaged by SRS with high specificity and little perturbation. The glucose transporter dependence of 3-OPG uptake was verified, and quantitative kinetics measurements showed the uptake of 3-OPG by cellular glucose transporters was fast and efficient. Simultaneous imaging of both 2-NBDG and 3-OPG showed little non-specific interaction of 3-OPG inside cells in contrast to 2-NBDG, supporting that 3-OPG can be a more truthful probe for glucose uptake. 3-OPG was further applied to visualize glucose uptake activity in live cancer cell lines, primary hippocampal neurons (Figure 4B), xenograft tumor tissues and mouse brain tissues to reveal heterogeneous patterns of uptake activity.

Besides glucose uptake by 3-OPG, isotopologues are used to investigate glucose incorporation. Bacterial species differentiation was demonstrated by coupling spontaneous Raman microscopy with ^{13}C-glucose[53]. The authors found that the ^{13}C-glucose incorporation shifted characteristic peaks to lower wavenumbers, which allows them to use multivariate methods subsequently for taxa discrimination. In another study[54, ^{13}C-glucose

incorporation into phenylalanine was probed as the stable isotope shifts the ring breathing mode to a unique frequency.

In addition to ^{13}C-glucose, D_7-glucose has also been coupled with SRS to study glucose metabolism and incorporation into de novo lipogenesis in single living cells[55] (Figure 4C and D). Unlike 3-OPG, D_7-glucose was shown to incorporate into cellular lipid synthesis by SRS imaging of C–D labeled lipid droplets. As expected, glucose utilization for lipid synthesis was found to be much larger in pancreatic cancer cells than normal pancreatic epithelial cells. In addition, compared to pancreatic cancer cells, prostate cancer cells had reduced de novo lipogenesis but higher activity of exogenous fatty acid uptake.

Small molecule drug imaging

The quantitative ability of SRS has made it an ideal tool to study drug uptake, distribution, delivery and screening. More importantly, the intrinsic or externally-introduced vibrational tags such as alkyne and nitrile can be used for improved chemical specificity and sensitivity without the problem of using bulky and perturbative fluorophores. Besides, the non-invasive nature of SRS makes it possible to image drugs in live cells or even live animal in real time.[56]

Drugs bearing nitrile or alkyne moiety can be readily imaged by SRS and Raman microscopy. Crawford *et al.* demonstrated SRS imaging of rhabduscin[57], a natural product by some gram-negative insect pathogens, which bears isonitrile as the intrinsic vibrational tag. In genetically transformed E. coli producing rhabduscin, they found significant rhabduscin localization in the cell periphery (Figure 4E and F). More recently, the sensitive property of nitrile to molecular structure was utilized to acquire structure-based imaging of protonated and deprotonated forms of carbonylcyanide p-trifluoromethoxyphenylhydrazone (FCCP) molecules in live cells with spontaneous Raman microscope[58] (Figure 4G and H). In another study, a series of diyne-tagged small mobile molecules coenzyme Q (CoQ) were synthesized and imaged in the mitochondria of live HeLa cells by line-scanned spontaneous Raman microscope[59] (Figure 4I and J). Two-color Raman imaging of EdU and diyne-tagged CoQ analogue AltQ2 were also demonstrated in live cells.

The subcellular localization of a drug contains useful information as some drugs target certain cellular compartments to function and some might be enriched in certain organelles that are not the designed targets. For example, label-free hyperspectral SRS imaging of two ABL1 tyrosine-kinase inhibitors imatinib and nilotinib has been achieved inside living cells. Both drugs were found to enrich in lysosomes for over 1000 fold due to the lysosomotropic properties.[60] Chloroquine was found to reduce the lysosomal trapping of imatinib, which suggests co-treatment with chloroquine may increase the drug efficacy through lysosome-mediated drug-drug interaction. In another study[61], erlotinib, an alkyne bearing FDA approved cancer drug was imaged with spontaneous Raman microscopy. The author found that the EGFR targeting drug is clustered with EGFR at membrane and induced receptor internalization.

SRS has also been applied to study drug delivery. The skin penetration pathway of alkyne-bearing drug terbinafine was visualized in mouse ear tissue by the 3D-sectioning of SRS[19]. The distribution of terbinafine matches with that of lipids, suggesting its delivery in tissues is through the lipid phase, consistent with its lipophilic property (Figure 4K–M).

In addition to the drug distribution and delivery, Raman scattering has been used for drug screening. Alkyne tag is recently applied to identify small molecule binding sites in protein.[62] The combination of alkyne tag and silver nanoparticles for SERS detection of peptide mixtures has demonstrated high sensitivity down to 100 femtomole. Alkyne-tag Raman screening (ATRaS) has successfully identified inhibitor-binding site in cysteine protease cathepsin B and is compatible with complex mixtures of trypsin-digested cell lysate.

Organelle imaging

Each organelle plays a specific and indispensable role in cellular processes. Fluorescent probes that can be targeted to specific organelles are capable of reporting localized bioinformation and are potentially useful for gaining insight in both healthy and diseased states of cells. Many fluorescent organelle probes have been developed by covalently incorporating an organelle-anchoring motif.[63, 64] However, the cytotoxicity, cell membrane permeability, non-specific interaction and photo-stability are the major issues in fluorescent organelle imaging.

A mitochondria-targeted vibrational tag has recently been reported by linking triphenylphosphonium with bisphenylbutadiyne, which exhibits strong Raman peak in the cell-silent region.[65] Line-scanning spontaneous Raman imaging of this tag has been demonstrated to visualize mitochondria in live cells. In addition, resonant Raman tags for organelle imaging were also developed recently based on quencher scaffold (azobenzene or blackberry quencher 650). These scaffolds have extremely low fluorescence and were modified to have red-shifted absorption for resonant Raman measurement.[66] And cell membrane, mitochondria and lysosome anchoring motifs were covalently linked to the quencher to allow organelle-specific imaging by resonant Raman imaging in live cells, although with limited imaging speed and sensitivity.

Brain imaging and metabolism

Ever since the invention of Golgi stain which makes it possible to see the whole nerve cell under microscopes, light microscopy has remained the key tool for neurobiologists to conduct structural and functional study in neurosystem for its noninvasive nature and high spatial-temporal resolution.[67] Voltage sensors and calcium sensors have been used to visualize voltage dynamics in the neurons; two-photon imaging and new laser-scanning approaches have been deployed to image deeper and faster; and super-resolution techniques have been applied to neurosciences which led to the discovery of new structural features.[68, 69] However, these techniques rely on fluorescence probes, which are generally difficult to label small molecules involved in the metabolism of neurosystems. SRS imaging of vibrational tags, on the other hand, provides an alternative contrast suitable for visualizing

cellular metabolism with high chemical specificity. Both deuterium substituted and alkyne tagged small molecules are successfully used for this purpose as reviewed in this section.

Synaptic plasticity is thought to be the cellular basis of learning and long-term memory formation, and changes in protein synthesis are required during the process. To visualize changes in proteins expression, Lu *et al.* applied deuterated amino acids to cultured hippocampal neurons[28]. By targeting carbon hydrogen bonds and carbon deuterium bonds respectively, they achieved ratiometric images between existing proteins and newly synthesized proteins, and identified newly grown neurites which had a higher percentage of newly synthesized proteins (Figure 5A). And in the follow-up study by the same group, where all 20 amino acids were replaced by their deuterium substituted counterparts in the custom-prepared media, the protein synthesis on an entire *ex vivo* organotypic brain slice was quantitatively visualized[29]. (Figure 5B) The authors found that the protein synthesis was only active in the dentate gyrus of the hippocampal region and in a few individual neurons. Given that the hippocampus is associated to long-term memory formation, this finding could hint the relationship between protein synthesis and neuronal plasticity.

In addition to protein, the metabolism of choline, an important small molecule of all living organisms for its structural and signaling functions, has also been demonstrated with deuterium substituted choline in hippocampal neurons. Hu *et al.* visualized the spatial distribution of choline metabolites in hippocampal neurons[40] (Figure 5C). In another study, propargylcholine was used to label choline species with higher signal intensity[19] (Figure 5D). In a recent study, acetylcholine, a neurotransmitter, was quantitatively imaged at neuromuscular junction of frog. The label-free imaging was achieved with frequency-modulated spectral-focusing stimulated Raman scattering microscopy that effectively removes imaging background.[11]

With all the tools developed for imaging nucleic acid, amino acids, fatty acid, and choline by SRS as previously described, Hu *et al.* further studied complex metabolism with all these vibrational tags in live rat brain hippocampal tissues and the metabolic response after traumatic injury with subcellular resolution[22]. In the dentate gyrus of hippocampus, they found heterogeneous incorporations of amino acids, choline and fatty acids at subcellular level. Interestingly, the suggestive neural progenitor cell division was also observed with pulse-chase labeling of ^{12}C and ^{13}C EdU isotopologues. In addition, they used the same platform to study the metabolic responses in live rat hippocampal tissues after traumatic injury, where they observed the elevated amino acid incorporation and lipid synthesis after mechanical injury (Figure 5E and F), hypothetically resulting from activating a cascade of anabolic metabolism for cell regeneration and neuron repair.

Conclusion

Reviewed above, vibrational tags coupled with SRS have become an essential tool that leads to new understanding in biological science. And as the chemical development of vibrational tags progresses for better tags with higher specificity, sensitivity and multiplex capability[70], while the instrumental[71] and algorithmic development advances for fast acquisition, hyperspectral modality and accurate classifiers, we can readily anticipate even broader

applications of the techniques, especially when small molecule metabolism is under investigation. For example, metabolic alterations are usually observed in cancer cells and might be a key to cancer proliferation and metastasis.[72] Meanwhile, metabolic heterogeneity is also a common phenomenon among cancer cells, influenced by factors including local environments and genetic diversity[73–75]. Therefore, it requires the chemical information for quantification of metabolic activity, as well as the temporal and spatial information to probe tumor metabolism. In this sense, SRS coupled with vibrational tags is an ideal tool for live cell imaging with high spatial-temporal resolution, and chemical specificity. In other areas such as neuroscience and clinical diagnostics, such combination has already and will continue to contribute to our frontier of knowledge.

Acknowledgments

We thank all the members of the Min group for contributions to this work. W.M. acknowledges support from an NIH Director's New Innovator Award (1DP2EB016573), R01 (EB020892), the US Army Research Office (W911NF-12-1-0594), the Alfred P. Sloan Foundation, and the Camille and Henry Dreyfus Foundation.

References

1. Milestones in light microscopy. Nature Cell Biology. 2009; 11(10):1165. [PubMed: 19794499]
2. Cheng J-X, Xie SX. Vibrational spectroscopic imaging of living systems: An emerging platform for biology and medicine. Science. 2015; 350(6264):aaa8870. [PubMed: 26612955]
3. Freudiger CW, Min W, Saar BG, Lu S, Holtom GR, He C, et al. Label-free biomedical imaging with high sensitivity by stimulated Raman scattering microscopy. Science. 2008; 322(5909):1857–61. [PubMed: 19095943]
4. Ploetz E, Laimgruber S, Berner S, Zinth W, Gilch P. Femtosecond stimulated Raman microscopy. Applied Physics B. 2007; 87(3):389–93.
5. Zhang C, Zhang D, Cheng J-X. Coherent Raman Scattering Microscopy in Biology and Medicine. Annual Review of Biomedical Engineering. 2014; 17(1):1–31.
6. Zhang D, Wang P, Slipchenko MN, Cheng J-X. Fast Vibrational Imaging of Single Cells and Tissues by Stimulated Raman Scattering Microscopy. Accounts of Chemical Research. 2014; 47(8):2282–90. [PubMed: 24871269]
7. Wei L, Hu F, Chen Z, Shen Y, Zhang L, Min W. Live-Cell Bioorthogonal Chemical Imaging: Stimulated Raman Scattering Microscopy of Vibrational Probes. Accounts of Chemical Research. 2016; 49(8):1494–502. [PubMed: 27486796]
8. Min W, Freudiger CW, Lu S, Xie XS. Coherent nonlinear optical imaging: beyond fluorescence microscopy. Annu Rev Phys Chem. 2011; 62:507–30. [PubMed: 21453061]
9. Evans CL, Xie SX. Coherent Anti-Stokes Raman Scattering Microscopy: Chemical Imaging for Biology and Medicine. Annual Review of Analytical Chemistry. 2008; 1(1):883–909.
10. Wakisaka Y, Suzuki Y, Iwata O, Nakashima A, Ito T, Hirose M, et al. Probing the metabolic heterogeneity of live Euglena gracilis with stimulated Raman scattering microscopy. Nature Microbiology. 2016; 1(10):16124.
11. Fu D, Yang W, Xie X. Label-free Imaging of Neurotransmitter Acetylcholine at Neuromuscular Junctions with Stimulated Raman Scattering. Journal of the American Chemical Society. 2016; 139(2):583–6. [PubMed: 28027644]
12. Lee H, Zhang D, Jiang Y, Wu X, Shih P-Y, Liao C-S, et al. Label-Free Vibrational Spectroscopic Imaging of Neuronal Membrane Potential. The Journal of Physical Chemistry Letters. 2017; 8(9): 1932–6. [PubMed: 28407470]
13. Ji M, Orringer DA, Freudiger CW, Ramkissoon S, Liu X, Lau D, et al. Rapid, Label-Free Detection of Brain Tumors with Stimulated Raman Scattering Microscopy. Science Translational Medicine. 2013; 5(201):201ra119.

14. Ji M, Lewis S, Camelo-Piragua S, Ramkissoon SH, Snuderl M, Venneti S, et al. Detection of human brain tumor infiltration with quantitative stimulated Raman scattering microscopy. Science Translational Medicine. 2015; 7(309):309ra163.
15. Orringer DA, Pandian B, Niknafs YS, Hollon TC, Boyle J, Lewis S, et al. Rapid intraoperative histology of unprocessed surgical specimens via fibre-laser-based stimulated Raman scattering microscopy. Nature Biomedical Engineering. 2017; 1(2):27.
16. Hu F, Chen Z, Zhang L, Shen Y, Wei L, Min W. Vibrational Imaging of Glucose Uptake Activity in Live Cells and Tissues by Stimulated Raman Scattering. Angewandte Chemie International Edition. 2015; 54(34):9821–5. [PubMed: 26207979]
17. Salic A, Mitchison TJ. A chemical method for fast and sensitive detection of DNA synthesis in vivo. Proceedings of the National Academy of Sciences. 2008; 105(7):2415–20.
18. Yamakoshi H, Dodo K, Okada M, Ando J, Palonpon A, Fujita K, et al. Imaging of EdU, an Alkyne-Tagged Cell Proliferation Probe, by Raman Microscopy. Journal of the American Chemical Society. 2011; 133(16):6102–5. [PubMed: 21443184]
19. Wei L, Hu F, Shen Y, Chen Z, Yu Y, Lin C-C, et al. Live-cell imaging of alkyne-tagged small biomolecules by stimulated Raman scattering. Nature Methods. 2014; 11(4):410–2. [PubMed: 24584195]
20. Hong S, Chen T, Zhu Y, Li A, Huang Y, Chen X. Live-Cell Stimulated Raman Scattering Imaging of Alkyne-Tagged Biomolecules. Angewandte Chemie. 2014; 126(23):5937–41.
21. Chen Z, Paley DW, Wei L, Weisman AL, Friesner RA, Nuckolls C, et al. Multicolor Live-Cell Chemical Imaging by Isotopically Edited Alkyne Vibrational Palette. Journal of the American Chemical Society. 2014; 136(22):8027–33. [PubMed: 24849912]
22. Hu F, Lamprecht MR, Wei L, Morrison B, Min W. Bioorthogonal chemical imaging of metabolic activities in live mammalian hippocampal tissues with stimulated Raman scattering. Scientific Reports. 2016; 6(1):39660. [PubMed: 28000773]
23. Jao CY, Salic A. Exploring RNA transcription and turnover in vivo by using click chemistry. Proceedings of the National Academy of Sciences. 2008; 105(41):15779–84.
24. Eden E, Geva-Zatorsky N, Issaeva I, Cohen A, Dekel E, Danon T, et al. Proteome Half-Life Dynamics in Living Human Cells. Science. 2011; 331(6018):764–8. [PubMed: 21233346]
25. Mann M. Functional and quantitative proteomics using SILAC. Nature Reviews Molecular Cell Biology. 2006; 7(12):952–8. [PubMed: 17139335]
26. Beatty KE, Liu JC, Xie F, Dieterich DC, Schuman EM, Wang Q, et al. Fluorescence Visualization of Newly Synthesized Proteins in Mammalian Cells. Angewandte Chemie International Edition. 2006; 45(44):7364–7. [PubMed: 17036290]
27. van Manen H-J, Lenferink A, Otto C. Noninvasive Imaging of Protein Metabolic Labeling in Single Human Cells Using Stable Isotopes and Raman Microscopy. Analytical Chemistry. 2008; 80(24):9576–82. [PubMed: 19006335]
28. Wei L, Yu Y, Shen Y, Wang MC, Min W. Vibrational imaging of newly synthesized proteins in live cells by stimulated Raman scattering microscopy. Proceedings of the National Academy of Sciences. 2013; 110(28):11226–31.
29. Wei L, Shen Y, Xu F, Hu F, Harrington JK, Targoff KL, et al. Imaging Complex Protein Metabolism in Live Organisms by Stimulated Raman Scattering Microscopy with Isotope Labeling. ACS Chemical Biology. 2015; 10(3):901–8. [PubMed: 25560305]
30. Shen Y, Xu F, Wei L, Hu F, Min W. Live-Cell Quantitative Imaging of Proteome Degradation by Stimulated Raman Scattering. Angewandte Chemie International Edition. 2014; 53(22):5596–9. [PubMed: 24737659]
31. Yu Y, Ramachandran PV, Wang MC. Shedding new light on lipid functions with CARS and SRS microscopy. Biochimica et Biophysica Acta (BBA) - Molecular and Cell Biology of Lipids. 2014; 1841(8):1120–9. [PubMed: 24576891]
32. Syed A, Smith EA. Raman Imaging in Cell Membranes, Lipid-Rich Organelles, and Lipid Bilayers. Annual Review of Analytical Chemistry. 2016; 10(1):1–21.
33. Maxfield FR, Tabas I. Role of cholesterol and lipid organization in disease. Nature. 2005; 438(7068):612–21. [PubMed: 16319881]

34. Maxfield FR, Wüstner D. Analysis of cholesterol trafficking with fluorescent probes. Methods in cell biology. 2012; 108:367–93. [PubMed: 22325611]
35. Matthäus C, Krafft C, Dietzek B, Brehm BR, Lorkowski S, Popp. Noninvasive Imaging of Intracellular Lipid Metabolism in Macrophages by Raman Microscopy in Combination with Stable Isotopic Labeling. Analytical Chemistry. 2012; 84(20):8549–56. [PubMed: 22954250]
36. Alfonso-García A, Pfisterer SG, Riezman H, Ikonen E, Potma EO. D38-cholesterol as a Raman active probe for imaging intracellular cholesterol storage. Journal of Biomedical Optics. 2016; 21(6):61003. [PubMed: 26719944]
37. Villareal VA, Fu D, Costello DA, Xie X, Yang PL. Hepatitis C Virus Selectively Alters the Intracellular Localization of Desmosterol. ACS Chemical Biology. 2016; 11(7):1827–33. [PubMed: 27128812]
38. Lee H, Zhang W, Zhang D, Yang Y, Liu B, Barker EL, et al. Assessing Cholesterol Storage in Live Cells and C. elegans by Stimulated Raman Scattering Imaging of Phenyl-Diyne Cholesterol. Scientific Reports. 2015; 5(1):7930. [PubMed: 25608867]
39. Holthuis J, Menon AK. Lipid landscapes and pipelines in membrane homeostasis. Nature. 2014; 510(7503):48–57. [PubMed: 24899304]
40. Hu F, Wei L, Zheng C, Shen Y, Min W. Live-cell vibrational imaging of choline metabolites by stimulated Raman scattering coupled with isotope-based metabolic labeling. Analyst. 2014; 139(10):2312–7. [PubMed: 24555181]
41. van Manen H-J, Kraan YM, Roos D, Otto C. Single-cell Raman and fluorescence microscopy reveal the association of lipid bodies with phagosomes in leukocytes. Proceedings of the National Academy of Sciences of the United States of America. 2005; 102(29):10159–64. [PubMed: 16002471]
42. Xie SX, Yu J, Yang W. Living Cells as Test Tubes. Science. 2006; 312(5771):228–30. [PubMed: 16614211]
43. Weeks T, Schie I, den Hartigh LJ, Rutledge JC, Huser T. Lipid-cell interactions in human monocytes investigated by doubly-resonant coherent anti-Stokes Raman scattering microscopy. Journal of Biomedical Optics. 2011; 16(2):21117.
44. Zhang D, Slipchenko MN, Cheng J-X. Highly Sensitive Vibrational Imaging by Femtosecond Pulse Stimulated Raman Loss. The journal of physical chemistry letters. 2011; 2(11):1248–53. [PubMed: 21731798]
45. Stiebing C, Meyer T, Rimke I, Matthäus C, Schmitt M, Lorkowski S, et al. Real-time Raman and SRS imaging of living human macrophages reveals cell-to-cell heterogeneity and dynamics of lipid uptake. Journal of Biophotonics. 2017
46. Fu D, Yu Y, Folick A, Currie E, Farese RV, Tsai T-H, et al. In Vivo Metabolic Fingerprinting of Neutral Lipids with Hyperspectral Stimulated Raman Scattering Microscopy. Journal of the American Chemical Society. 2014; 136(24):8820–8. [PubMed: 24869754]
47. Plathow C, Weber WA. Tumor Cell Metabolism Imaging. Journal of Nuclear Medicine. 2008; 49(Suppl 2):43S–63S. [PubMed: 18523065]
48. Walker-Samuel S, Ramasawmy R, Torrealdea F, Rega M, Rajkumar V, Johnson PS, et al. In vivo imaging of glucose uptake and metabolism in tumors. Nature Medicine. 2013; 19(8):1067–72.
49. O'Neil RG, Wu L, Mullani N. Uptake of a Fluorescent Deoxyglucose Analog (2-NBDG) in Tumor Cells. Molecular Imaging and Biology. 2005; 7(6):388–92. [PubMed: 16284704]
50. Yamada K, Saito M, Matsuoka H, Inagaki N. A real-time method of imaging glucose uptake in single, living mammalian cells. Nature Protocols. 2007; 2(3):753–62. [PubMed: 17406637]
51. Zanetti-Domingues LC, Tynan CJ, Rolfe DJ, Clarke DT, Martin-Fernandez M. Hydrophobic Fluorescent Probes Introduce Artifacts into Single Molecule Tracking Experiments Due to Non-Specific Binding. PLoS ONE. 2013; 8(9):e74200. [PubMed: 24066121]
52. Hughes LD, Rawle RJ, Boxer SG. Choose Your Label Wisely: Water-Soluble Fluorophores Often Interact with Lipid Bilayers. PLoS ONE. 2014; 9(2):e87649. [PubMed: 24503716]
53. Huang WE, Griffiths RI, Thompson IP, Bailey MJ, Whiteley AS. Raman Microscopic Analysis of Single Microbial Cells. Analytical Chemistry. 2004; 76(15):4452–8. [PubMed: 15283587]

54. Venkata H, Shigeto S. Stable Isotope-Labeled Raman Imaging Reveals Dynamic Proteome Localization to Lipid Droplets in Single Fission Yeast Cells. Chemistry & Biology. 2012; 19(11): 1373–80. [PubMed: 23177192]
55. Li J, Cheng J-X. Direct Visualization of De novo Lipogenesis in Single Living Cells. Scientific Reports. 2014; 4(1):6807. [PubMed: 25351207]
56. Tipping WJ, Lee M, Serrels A, Brunton VG, Hulme AN. Stimulated Raman scattering microscopy: an emerging tool for drug discovery. Chemical Society Reviews. 2016; 45(8):2075–89. [PubMed: 26839248]
57. Crawford JM, Portmann C, Zhang X, Roeffaers MBJ, Clardy J. Small molecule perimeter defense in entomopathogenic bacteria. Proceedings of the National Academy of Sciences. 2012; 109(27): 10821–6.
58. Yamakoshi H, Palonpon AF, Dodo K, Ando J, Kawata S, Fujita K, et al. Simultaneous imaging of protonated and deprotonated carbonylcyanide p -trifluoromethoxyphenylhydrazone in live cells by Raman microscopy. Chemical Communications. 2013; 50(11):1341–3.
59. Yamakoshi H, Dodo K, Palonpon A, Ando J, Fujita K, Kawata S, et al. Alkyne-Tag Raman Imaging for Visualization of Mobile Small Molecules in Live Cells. Journal of the American Chemical Society. 2012; 134(51):20681–9. [PubMed: 23198907]
60. Fu D, Zhou J, Zhu W, Manley PW, Wang KY, Hood T, et al. Imaging the intracellular distribution of tyrosine kinase inhibitors in living cells with quantitative hyperspectral stimulated Raman scattering. Nature Chemistry. 2014; 6(7):614–22.
61. El-Mashtoly SF, Petersen D, Yosef HK, Mosig A, Reinacher-Schick A, Kötting C, et al. Label-free imaging of drug distribution and metabolism in colon cancer cells by Raman microscopy. Analyst. 2013; 139(5):1155–61.
62. Ando J, Asanuma M, Dodo K, Yamakoshi H, Kawata S, Fujita K, et al. Alkyne-tag SERS screening and identification of small-molecule-binding sites in protein. Journal of the American Chemical Society. 2016; 138(42):13901–10.
63. Xu W, Zeng Z, Jiang JH, Chang YT, Yuan L. Discerning the Chemistry in Individual Organelles with Small-Molecule Fluorescent Probes. Angewandte Chemie International Edition. 2016; 55(44):13658–99. [PubMed: 27571316]
64. Zhu H, Fan J, Du J, Peng X. Fluorescent Probes for Sensing and Imaging within Specific Cellular Organelles. Accounts of Chemical Research. 2016; 49(10):2115–26. [PubMed: 27661761]
65. Yamakoshi H, Palonpon A, Dodo K, Ando J, Kawata S, Fujita K, et al. A sensitive and specific Raman probe based on bisarylbutadiyne for live cell imaging of mitochondria. Bioorganic & Medicinal Chemistry Letters. 2015; 25(3):664–7. [PubMed: 25522818]
66. Kuzmin AN, Pliss A, Lim C-K, Heo J, Kim S, Rzhevskii A, et al. Resonance Raman Probes for Organelle-Specific Labeling in Live Cells. Scientific Reports. 2016; 6(1):28483. [PubMed: 27339882]
67. Wilt BA, Burns LD, Wei Ho ET, Ghosh KK, Mukamel EA, Schnitzer MJ. Advances in light microscopy for neuroscience. Annu Rev Neurosci. 2009; 32:435–506. [PubMed: 19555292]
68. Combs CA. Fluorescence microscopy: a concise guide to current imaging methods. Curr Protoc Neurosci. 2010; Chapter 2(Unit 2):1.
69. Svoboda K, Yasuda R. Principles of two-photon excitation microscopy and its applications to neuroscience. Neuron. 2006; 50(6):823–39. [PubMed: 16772166]
70. Wei L, Chen Z, Shi L, Long R, Anzalone AV, Zhang L, et al. Super-multiplex vibrational imaging. Nature. 2017; 544(7651):465–70. [PubMed: 28424513]
71. CH, Lee Y, Heddleston JM, Hartshorn CM, Walker AR, Rich JN, et al. High-speed coherent Raman fingerprint imaging of biological tissues. Nature Photonics. 2014; 8(8):627–34. [PubMed: 25621002]
72. Cairns RA, Harris IS, Mak TW. Regulation of cancer cell metabolism. Nature Reviews Cancer. 2011; 11(2):85–95. [PubMed: 21258394]
73. Sengupta D, Pratx G. Imaging metabolic heterogeneity in cancer. Molecular Cancer. 2015; 15(1): 1–12.
74. Coloff JL, Brugge JS. Metabolic changes promote rejection of oncogenic cells. Nature Cell Biology. 2017; 19(5):414–5. [PubMed: 28446818]

75. McGranahan N, Swanton C. Clonal Heterogeneity and Tumor Evolution: Past, Present, and the Future. Cell. 2017; 168(4):613–28. [PubMed: 28187284]

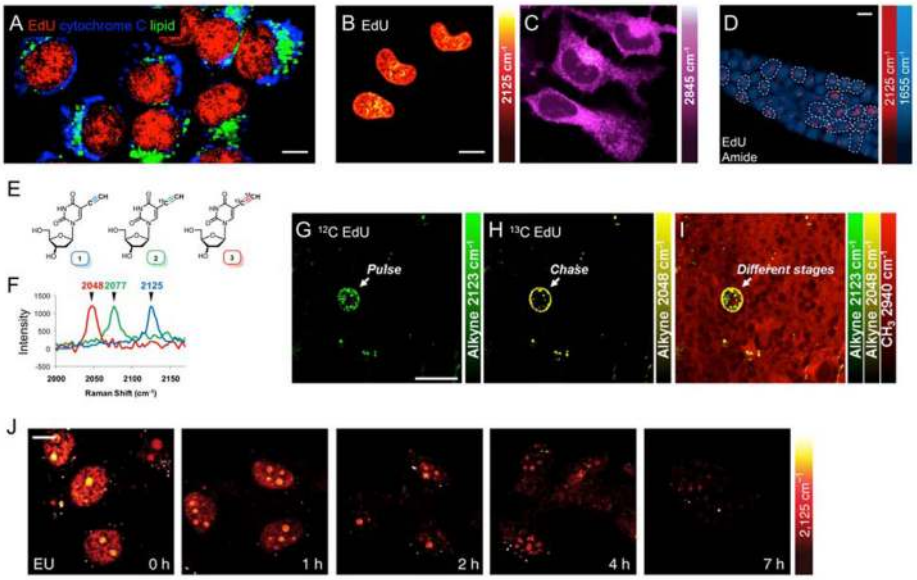

Figure 1. Raman images of nucleic acids

(A) Raman spectral imaging of HeLa cells labeled with EdU[18]. Scale bar: 10 μm. (B and C) SRS imaging of alkyne (B) and lipid (C) channel of HeLa cells labeled with EdU[19]. Scale bar: 10 μm. (D) SRS imaging of EdU reveals cell proliferation in C elegans[19]. Scale bar: 5 μm. (E and F) structures and Raman spectra of isotope-edited EdU molecules[21]. (G to I) SRS imaging of ^{12}C-EdU (G) ^{13}C-EdU (H) channels and their overlay (I) in a pulse chase labeled neuron progenitor cell[22]. Scale bar: 20 μm. (J) SRS imaging reveals the decay of alkyne signal following pulse labeling of EU in cells[19]. Scale bar: 10 μm.

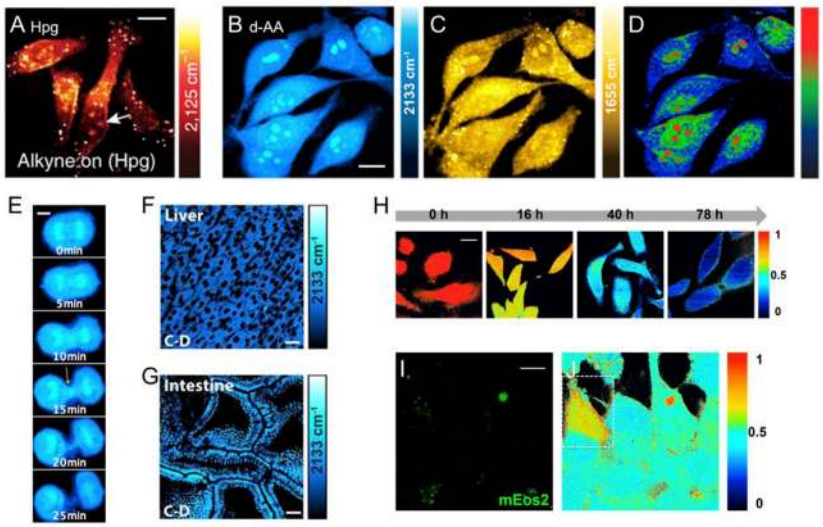

Figure 2. Visualization of protein metabolism with vibrational tags

(A) SRS imaging of alkyne from HeLa cells labeled with Hpg[19]. Scale bar: 10 μm. (B to D) SRS imaging of C–D channel (B), amide channel (C), and ratiometric (D) images of HeLa cells labeled with deuterated amino acids[28]. Scale bar: 10 μm. (E) time-lapse imaging of HeLa cells labeled with deuterated amino acids during cytokinesis, arrow indicates newly synthesized proteins at mid-body[28]. Scale bar: 10 μm. (F and G) SRS imaging of newly synthesized proteins in liver. (F) and intestine (G) tissue sections of mouse after administration of deuterated amino acid[29]. Scale bar: 10 μm. (H) SRS ratiometric imaging of ^{12}C- and ^{13}C-phenylalanine can be used to quantify protein turnover in HeLa cells[30]. Scale bar: 20 μm. (I) Cells with a fluorescent marker indicate the localization of poly-Q protein aggregate. (J) Phenylalanine ratiometric imaging of same cell in (I) indicates heterogeneity in protein turnover[30]. Scale bar: 10 μm.

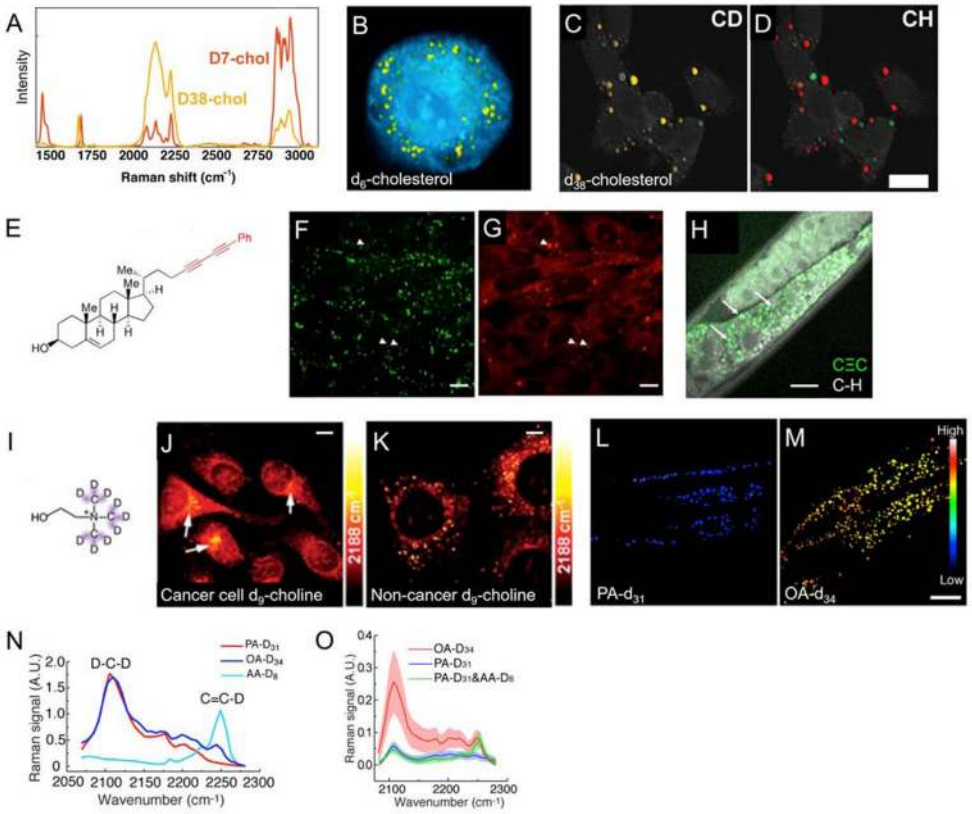

Figure 3. Lipid metabolism visualized by isotopologues vibrational tags

(A) Comparison of C–D Raman intensity in D_7-cholesterol and D_{38}-cholesterol[36]. (B) Spontaneous Raman imaging of d_6-cholsterol scavenged into LDs of macrophage cell[35]. (C and D) Hyperspectral SRS imaging reveals heterogeneous d38-cholesterol incorporation into LD populations (C), which correlates with distinct hyper spectral features in C–H vibration (D)[36]. Scale bar: 20 μm. (E) Structure of phenyldiyne-tagged cholesterol[38]. (F and G) SRS imaging of phenyldiyne-cholesterol (F) and BODIPY staining (G) in M12 cells reveals cholesterol accumulation into both LDs and lysosomes[38]. Scale bar: 10 μm. (H) SRS imaging of phenyldiyne-cholesterol in C elegans[38]. Scale bar: 10 μm. (I) Structure of D_9-choline molecule[40]. (J and K) Comparison of D_9-choline incorporation between cancer cell (J) and non-cancer cell (K) reveals elevated choline metabolism in cancer cells[40]. Scale bar: 10 μm (L and M) Hyperspectral SRS imaging reveals difference between incorporation rate (C–D/C–H) of PA-d_{31} (L) and OA-d_{31} (M)[46]. Scale bar: 20 μm. (N) SRS spectra of different fatty acids[46]. (O) Metabolic profiling in LDs reveals distinct spectral features after incorporation of different fatty acids[46].

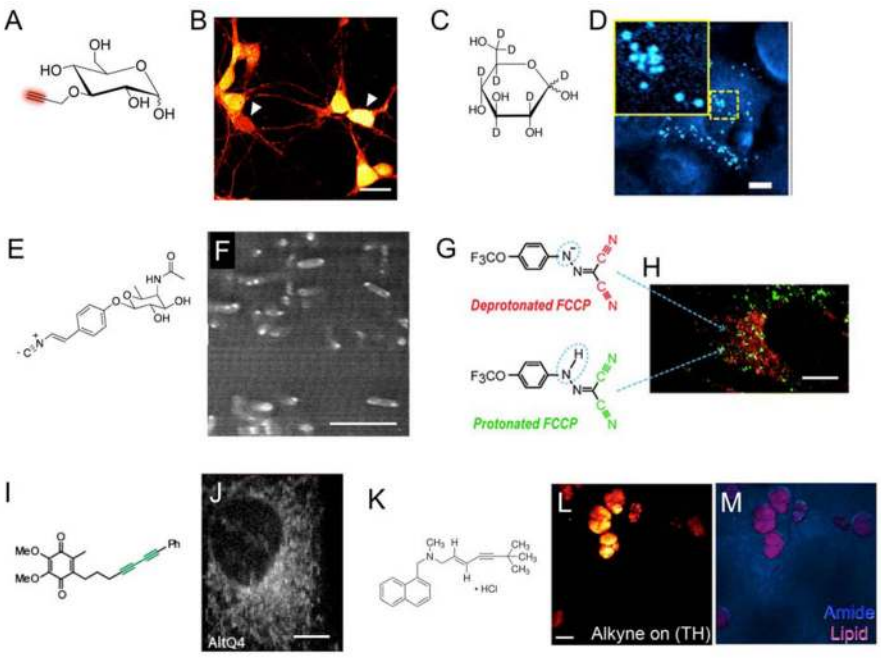

Figure 4. Raman images of glucose and small molecule drugs bearing vibrational tags

(A and B) Structure and SRS imaging of an alkyne-tagged glucose analog, 3-OPG[16]. Scale bar: 40 μm. (C and D) structure of d_7-glucose and SRS imaging of de novo lipogenesis from d_7-glucose[55]. Scale bar: 10 μm. (E) Structure of Rhabduscin. (F) SRS imaging of isonitrile reveals the distribution of Rhabduscin in cell periphery of X. nematophila[57]. Scale bar: 10 μm. (G and H) Deprotonated (upper) and protonated (bottom) forms of FCCP (G) and Raman imaging of their distribution in HeLa cell (H)[58]. Scale bar: 10 μm. (I) Structure of a phenyldiyne-tagged CoQ (AltQ4). (J) Raman imaging of AltQ4 accumulation in HeLa cell[59]. Scale bar: 10 μm. (K) structure of terbinafine, a skin drug[19]. (L and M) SRS images at alkyne, amide and lipid channel[19]. Scale bar: 20 μm.

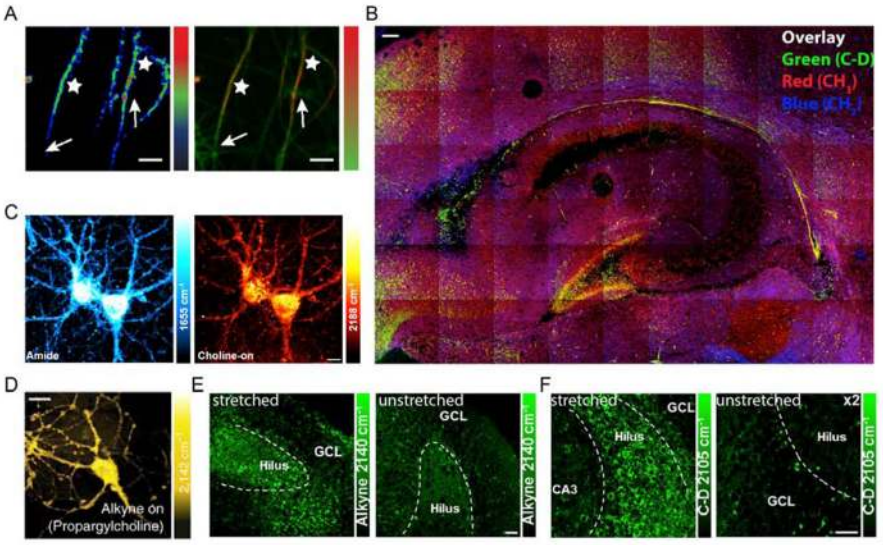

Figure 5. SRS images of cultured neurons and brain slides with isotopologues and alkyne tags

(A) left:Ratio image between new protein and total proteins. Although the starred neurites show high percentage of new proteins, the arrows indicate neurites displaying very low new protein percentage. right: Merged image between new protein (red channel) and total proteins (green channel). Similarly, the starred regions show obvious new proteins, whereas the arrows indicate regions that have undetectable new protein signal[28]. Scale bar: 10 μm. (B) A 4 × 3 mm^2 large-field view overlay image of new proteins (C–D, green), old proteins (CH3, red), and total lipids (CH_2, blue) for a brain slice (400 μm thick, from a P12 mouse)[29]. Scale bar, 100 μm. (C) Image of a single neuron shows the subcellular distribution of D_9-choline metabolites. The amide images (left) display the same set of cells as in the choline-on images (right)[40]. Scale bar: 10 μm. (D) Live neurons incubated with propargylcholine[19]. Scale bar: 10 μm. (E–F) Increased choline (E) and fatty acid (F) metabolism for lipid synthesis are observed in the hilus of dentate gyrus after mechanical stretch[22]. Scale bars: 40 μm.